ARTICLE

Prediction on Failure Pressure of Pipeline Containing Corrosion Defects Based on ISSA-BPNN Model

Qi Zhuang[1,*], Dong Liu[2] and Zhuo Chen[3]

[1]PetroChina Changqing Oilfield Company, The Second Gas Production Plant, Xi'an, 710000, China

[2]PetroChina Changqing Oilfield Company, Safety and Environmental Supervision Department Co., Ltd., Xi'an, 710000, China

[3]Sinopec Northwest Oilfield Company, The Second Oil Production Plant Co., Ltd., Urumqi, 830016, China

[*]Corresponding Author: Qi Zhuang. Email: zhuangqi1210@163.com

ABSTRACT

Oil and gas pipelines are affected by many factors, such as pipe wall thinning and pipeline rupture. Accurate prediction of failure pressure of oil and gas pipelines can provide technical support for pipeline safety management. Aiming at the shortcomings of the BP Neural Network (BPNN) model, such as low learning efficiency, sensitivity to initial weights, and easy falling into a local optimal state, an Improved Sparrow Search Algorithm (ISSA) is adopted to optimize the initial weights and thresholds of BPNN, and an ISSA-BPNN failure pressure prediction model for corroded pipelines is established. Taking 61 sets of pipelines blasting test data as an example, the prediction model was built and predicted by MATLAB software, and compared with the BPNN model, GA-BPNN model, and SSA-BPNN model. The results show that the $MAPE$ of the ISSA-BPNN model is 3.4177%, and the R^2 is 0.9880, both of which are superior to its comparison model. Using the ISSA-BPNN model has high prediction accuracy and stability, and can provide support for pipeline inspection and maintenance.

Nomenclature

P_F	Experimental value of pipeline failure pressure
$\hat{P}_F$	Predicted value of pipeline failure pressure
R_e	Relative error

1 Introduction

As the fifth largest transportation mode after highway, railway, water, and air transportation, pipeline transportation plays an important role in oil and natural gas transportation because of its advantages such as large transportation capacity, economy and environmental protection, low energy consumption, and not easy to be restricted by external conditions [1]. By 2022, the mileage of newly built oil and gas pipelines in China is about 4,668 kilometers, and the total mileage of oil and gas pipelines has reached 155,000 kilometers [2]. Pipeline failure will cause huge losses to enterprises and

society, and corrosion is one of the main reasons for pipeline failure [3–5]. Therefore, it is of great significance to study the failure pressure of corrosion defect pipelines to ensure the pipeline's safe operation.

Scholars at home and abroad have studied the failure pressure prediction model of oil and gas pipelines, for example, the AGA Pipeline Research Committee proposed NG-18 circumferential failure stress calculation formula based on fracture mechanics, Kiefner and others proposed B31G criterion for residual strength calculation of single corrosion defect, and ASME revised it several times later, the most commonly used version is ASME B31G-2009 [6]. It also has the LPC criterion by British Gas, the PCORRC criterion by Battelle, and the DNV-RP-F101 standard by British Gas and the Norwegian classification society DNV [7–9]. However, the above-mentioned traditional forecasting models are conservative and have low accuracy, which has certain limitations. Some Chinese scholars use the ANSYS finite element analysis method to establish prediction models for pipelines with different corrosion degrees to predict pipeline failure pressure [10,11]. This method can build prediction models according to the actual characteristics of pipelines and failure criteria in different environments, but the calculation process is complicated and is not conducive to prediction.

In recent years, with the development of computer and intelligent algorithms, the research of pipeline failure pressure prediction models has been more inclined to computer-intelligent algorithms. Liu et al. [12] predicted the residual strength of a defective pipeline based on the Support Vector Machine (SVM) algorithm. Jiang et al. [13] established a hybrid prediction model based on support vector regression (SVR) and Particle Swarm Optimization (PSO). Some scholars predicted the residual strength of defective pipelines based on the Extreme Learning Machine (ELM) algorithm [14]. Most scholars established the prediction model of pipeline failure pressure based on the BP neural network [15,16].

To sum up, only a few scholars based on the ELM algorithm of pipeline failure pressure prediction model, the accuracy of the ELM model is about 11%. Most scholars have established pipeline failure pressure prediction models based on the BP neural network, the accuracy of the BPNN model is about 10%. Li et al. [17] used ABAQUS and MATLAB to analyze the failure pressure of pipelines with axial double corrosion defects in cold areas, proving the BPNN model is accurate in predicting failure pressure. This paper also establishes a prediction model of pipeline failure pressure based on the BP neural network. Because the BP neural network adopts error backpropagation training, it needs many iterations to get the optimal model parameters, and the convergence rate is usually slow. Therefore, this paper introduces a Logistic chaotic map to propose an ISSA algorithm, to further improve the accuracy and stability of the BP neural network model prediction, and provide technical support for failure pressure prediction and safety management of corroded pipelines.

2 BPNN and Optimization Algorithm

2.1 BPNN Model

BPNN is a multi-layer feedforward network, which consists of an input layer, a hidden layer, and an output layer, the network structure diagram is shown in Fig. 1 [18]. The learning process of BP neural network includes two stages: forward propagation of signal and back propagation of error. In the first stage, the network input signal is transferred from the input layer to the hidden layer, and then transferred to the output layer after the activation operation of the hidden layer activation function. After the hidden layer activation function, the output of the hidden layer can be controlled in the range of 0~1, and then transferred to the output layer. In the second stage, the network carries out back propagation according to the error comparison between the predicted value and the experimental

value. By adjusting the weights and thresholds between neurons, the whole network can be corrected continuously in the direction of error reduction.
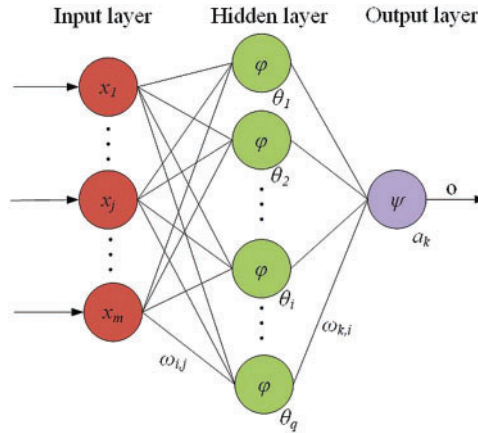

Figure 1: BP neural network structure diagram

2.2 SSA Optimization Algorithm and Its Improvement

2.2.1 SSA Optimization Algorithm

In 2020, Xue et al. [19] proposed SSA inspired by sparrows' foraging behavior and anti-predation behavior. The algorithm divides all individuals of a sparrow population into two roles: discoverer and participant. Among them, the discoverer has a higher energy reserve and is responsible for finding foraging places with more food. The participants had lower energy reserves, but they were always able to find the finder who provided the best food source and then came close to competing for food. The energy reserve of the sparrow individual is represented by Fitness Value in the actual modeling process. In the whole sparrow population, some sparrows are always aware of the appearance of predators. This part of the sparrow accounts for 10% to 20% of the total population, and this part of the sparrow is called the guard. Discoverers and participants can change roles with each other, but it is necessary to ensure that the proportion of discoverers and participants in the whole population remains unchanged.

In the process of solving the actual d-dimensional problem to be optimized by SSA, the population composed of n sparrows is set as:

$$X = \begin{pmatrix} x_{1,1} & \cdots & x_{1,d} \\ \vdots & \ddots & \vdots \\ x_{n,1} & \cdots & x_{n,d} \end{pmatrix} \tag{1}$$

The fitness value of the whole sparrow population can be expressed as:

$$F_X = \begin{bmatrix} f\left([x_{1,1} \cdots x_{1,d}]\right) \\ \vdots \\ f\left([x_{n,1} \cdots x_{n,d}]\right) \end{bmatrix} \tag{2}$$

where: f represents the fitness value of a single sparrow in the population.

In the actual search process, according to the rules, the update of the finder position in the population is described by the following Eq. (3):

$$X_{i,j}^{t+1} = \begin{cases} X_{i,j}^t \cdot \exp\left(-\dfrac{i}{\alpha \cdot iter_{\max}}\right) & if\ R_2 < ST \\ X_{i,j}^t + Q \cdot L & if\ R_2 \geq ST \end{cases} \tag{3}$$

where: t represents the current iteration algebra, $j = 1, 2, 3, \ldots, d$. $X_{i,j}$ represents the position information of the i-th sparrow in the j-th dimension. α is a random number between (0, 1). $iter_{max}$ represents the maximum number of iterations. R_2 ($R_2 \in [0, 1]$) indicates the warning value, ST ($ST \in [0.5, 1]$) denotes safe values. Q is a random number and obeys normal distribution. L is a matrix with dimensions $1 \times d$, where each element is 1.

According to the predator rule, the update of the participant position is described by the following Eq. (4):

$$X_{i,j}^{t+1} = \begin{cases} Q \cdot \exp\left(\dfrac{X_{worst} - X_{i,j}^t}{i^2}\right) & if\ i > n/2 \\ X_p^{t+1} + \left|X_{i,j}^t - X_p^{t+1}\right| \cdot A^+ \cdot L & otherwise \end{cases} \tag{4}$$

where: X_p represents the ideal food source position found by the current discoverer, and X_{worst} denotes the current overall worst position. The entries of matrix A, which has dimensions of $1 \times d$, are randomly assigned to either 1 or -1, and satisfies $A^+ = A^T \left(AA^T\right)^{-1}$.

The initial position of the guard is randomly generated in the population, and the update of its position is described by the following Eq. (5):

$$X_{i,j}^{t+1} = \begin{cases} X_{best}^t + \beta \cdot \left|X_{i,j}^t - X_{best}^t\right| & if\ f_i > f_g \\ X_{i,j}^t + K \cdot \left(\dfrac{\left|X_{i,j}^t - X_{worst}^t\right|}{(f_i - f_w) + \varepsilon}\right) & if\ f_i = f_g \end{cases} \tag{5}$$

where: X_{best} is the best food source location at present. K and β are step size control parameters, and β is a random number with the normal distribution of mean value 0 and variance 1; K is a random number over [1,1] and also indicates the direction in which the sparrow moves. f_i, f_g and f_w are the current individual, global best, and worst fitness values, respectively. ε is the minimum constant set to avoid zero denominators.

2.2.2 ISSA Optimization Algorithm by Logistic Chaotic Map

A common example of a chaotic map is the logistic chaotic map. It is extensively utilized because of its straightforward mathematical form [20]. In this paper, based on a Logistic chaotic map, an improved sparrow algorithm is proposed, which optimizes the initial population. Its mathematical expression is:

$$Y_{n+1} = a Y_n (1 - Y_n) \tag{6}$$

where: $Y_n \in [0, 1]$, $a \in [0, 4]$ is the Logistic parameter.

The closer a is to 4, the more the range of Y is evenly distributed to the whole [0,1] region. When a is 4, the system is in a completely chaotic state, and the uniformity of mapping distribution reaches the extreme value, so the value of a is 4 in this paper.

3 Modeling and Evaluation

3.1 Model Building

When improving the SSA Optimization Algorithm, the Logistic chaotic map strategy is mainly used to initialize the population. The flow of ISSA-BP prediction model is shown in Fig. 2.

(1) Using a Logistic mapping strategy to initialize population, and iteration times and initialize the proportion of discoverer and participant.

(2) Calculate and arrange fitness values.

(3) Update the discoverer's location.

(4) Update the participant's location.

(5) Update the guard's location.

(6) Calculate the fitness value and update the sparrow position.

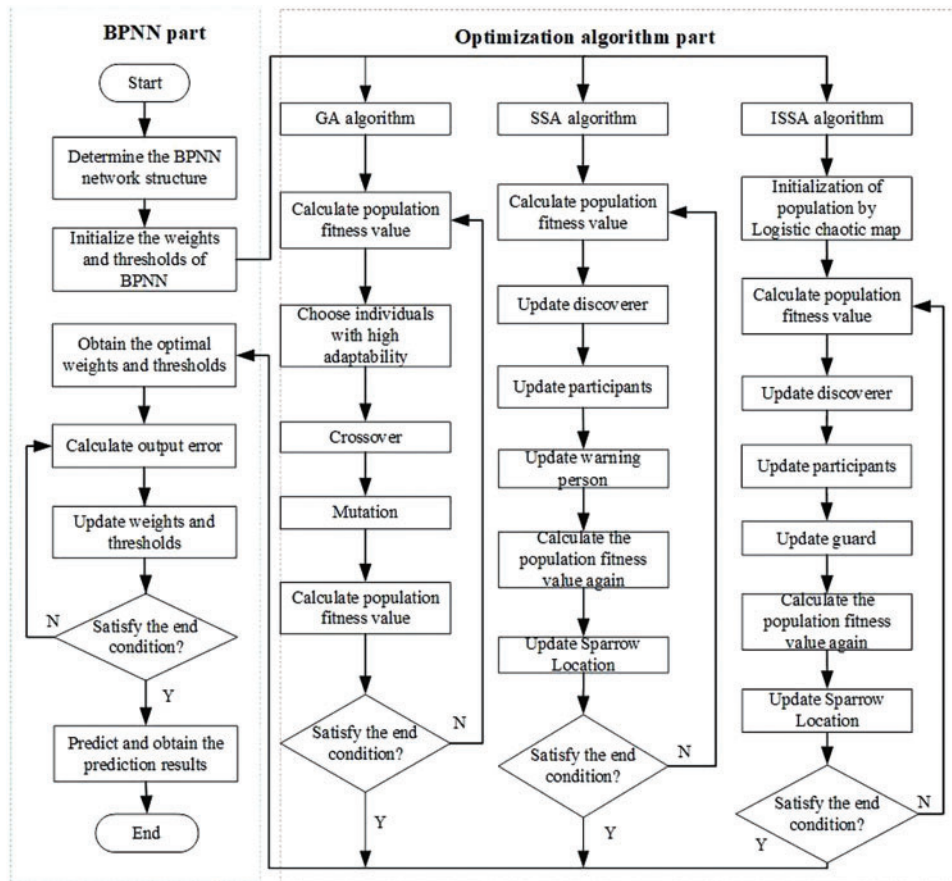(7) If the termination condition is satisfied, end and output the result; otherwise, repeat steps 2–6.

Figure 2: Flowchart of the optimized mode

3.2 Evaluation Indicators

To evaluate the prediction effect, mean absolute error (MAE), root mean square error ($RMSE$), mean absolute percentage error ($MAPE$), and determination coefficient R^2 were selected as evaluation

indexes. The smaller the values of MAE, $RMSE$, and $MAPE$, and the larger the values of R^2, the higher the prediction accuracy of the model. It is described by the following Eqs. (7)–(10):

$$MAE = \frac{1}{N} \sum_{i=1}^{N} \left| P_F - \hat{P}_F \right| \tag{7}$$

$$RMSE = \sqrt{\frac{1}{N} \sum_{i=1}^{N} \left(P_F - \hat{P}_F \right)^2} \tag{8}$$

$$MAPE = \frac{1}{N} \sum_{i=1}^{N} \left| \frac{P_F - \hat{P}_F}{P_F} \right| \times 100\% \tag{9}$$

$$R^2 = 1 - \frac{\sum_{i=1}^{n} \left(P_F - \hat{P}_F \right)^2}{\sum_{i=1}^{n} \left(P_F - \bar{P}_F \right)^2} \tag{10}$$

where: P_F is the experimental value of pipeline failure pressure; $\hat{P}_F$ is the predicted value of pipeline failure pressure; $\bar{P}_F$ is the average value of the experimental value of pipeline failure pressure; N is the total number of test samples.

4 Example Analysis

4.1 Data Acquisition

61 groups of experimental data of pipe blasting with defects are selected in reference [9]. Each group of data includes 8 types: Pipe outer diameter, Wall thickness, Defect length, Defect depth, Defect width, Yield strength, Tensile strength, and Failure pressure. 45 groups of data are randomly selected for learning and training, and the remaining 16 groups of data are used to verify the prediction effect of the model. The experimental data of pipeline blasting with defects are shown in Table 1.

Table 1: Data of blasting tests on pipelines containing defects

Number	Pipe outer diameter /mm	Wall thickness /mm	Defect length /mm	Defect depth /mm	Defect width /mm	Yield strength /MPa	Tensile strength /MPa	Failure pressure /MPa
1	459.4	8	40.05	3.75	32	589	730.5	24.2
2	323.9	9.71	350	6.93	95.3	452	542	13.58
3	508	14.6	500	10.35	97	478	600	14.6
4	76.2	2	75	1.4	16	391	458	9.4
5	76.2	2.04	75	1.44	16	260	309	5.45
6	508	6.35	900	2.16	25.4	540	610.3	11.8
7	762	17.5	900	8.75	50	495	565	15
8	762	17.5	200	4.2	50	474.1	556.6	24.11
9	762	17.5	200	8.9	50	474.1	556.6	21.76

(Continued)

Table 1 (continued)

Number	Pipe outer diameter /mm	Wall thickness /mm	Defect length /mm	Defect depth /mm	Defect width /mm	Yield strength /MPa	Tensile strength /MPa	Failure pressure /MPa
10	762	17.5	200	13.1	50	474.1	556.6	17.15
11	762	17.5	100	8.4	50	474.1	556.6	24.3
12	762	17.5	300	8.5	50	474.1	556.6	19.8
13	762	17.5	200	8.4	100	474.1	556.6	23.42
14	762	17.5	200	9	200	474.1	556.6	22.64
15	426	6.95	160	2.7	25	240	390	10.8
16	426	7	150	3.8	21	240	390	9.81
17	426	7	150	5.2	25	240	390	7.85
18	529	9	350	4.7	25	285	415	8.83
19	529	9	160	4.7	25	285	415	15.7
20	529	9	150	5.3	25	285	415	14.2
21	720	8	180	4.3	25	425	535	10.3
22	720	8	320	4.4	26	425	535	8.83
23	720	8	180	6.2	26	425	535	7.55
24	304.8	6.35	26	4.95	20	351	543	15.36
25	304.8	6.35	33	4.25	21	382	570	16.29
26	304.8	6.35	37	4.64	30	351	463	14.29
27	324	6.01	19.35	3.6	19	382	570	16.22
28	324	10.3	243	5.15	154.9	380	514	23.2
29	324	10.3	243	5.15	30.9	380	514	22
30	508	6.6	381	2.62	25.4	443.4	598.9	11.25
31	508	6.35	900	3.43	25.4	429.6	572.5	8
32	508	6.35	1000	3.18	25.4	434.8	572.5	8.4
33	508	6.7	1016	2.66	25.4	430	601	11.55
34	323.9	9.8	255.6	6.95	95.3	422.5	589.6	11.4
35	323.9	9.71	350	6.85	95.3	422.5	589.6	13.58
36	323.9	9.91	433.4	7.08	95.3	422.5	589.6	12.19
37	323.9	9.74	527.8	7.06	95.3	422.5	589.6	11.3
38	1422.4	19.25	180	10.4	0.5	740	774	15.35
39	1422.4	20.1	385	3.8	0.5	795	840	20.12
40	914.4	16.4	150	9	0.5	739	813	21.4
41	914.4	16.4	450	6	0.5	739	813	24.02
42	458.8	8.1	39.6	5.39	31.9	601	684	22.68
43	323.9	9.8	255.6	7.08	95.3	452	542	14.4
44	323.9	9.66	305.6	6.76	95.3	452	542	14.07
45	323.9	9.71	394.5	6.91	95.3	452	542	12.84
46	323.9	9.91	433.4	7.31	95.3	452	542	12.13
47	323.9	9.74	466.7	7.02	95.3	452	542	11.92
48	323.9	9.79	488.7	6.99	95.3	452	542	11.91

(Continued)

Table 1 (continued)

Number	Pipe outer diameter /mm	Wall thickness /mm	Defect length /mm	Defect depth /mm	Defect width /mm	Yield strength /MPa	Tensile strength /MPa	Failure pressure /MPa
49	323.9	9.79	500	6.99	95.3	452	542	11.99
50	323.9	9.74	527	7.14	95.3	452	542	11.3
51	508	14.3	500	10.3	97	478	600	13.4
52	508	14.8	500	9.7	97	478	600	15.8
53	508	6.6	381	2.62	25.4	540	610.3	11.25
54	508	6.35	900	3.43	25.4	540	610.3	8
55	508	6.35	1000	3.18	25.4	540	610.3	8.4
56	508	6.7	1016	2.66	25.4	540	610.3	11.55
57	762	17.5	50	8.75	50	495	565	27.5
58	762	17.5	100	8.75	50	495	565	24.3
59	762	17.5	200	8.75	50	495	565	21.8
60	762	17.5	300	8.75	50	495	565	19.8
61	762	17.5	600	8.75	50	495	565	16.5

4.2 Model Parameter Setting

4.2.1 BPNN Model Parameter Setting

BPNN model adopt a three-layer network structure, with training times of 1000, a learning rate of 0.01, and a minimum error of training target of 0.0001. The network input layer is the factors that affect the failure pressure of the pipeline, so the number of neurons in the input layer is 7; The output layer is pipeline failure pressure, so the number of neurons in the output layer is 1; The hidden layer's neuronal number is determined according to Eq. (11). The optimal hidden layer's neuronal number is determined by the trial value, and the trial value results are shown in Fig. 3.

$$H = \sqrt{m+n} + a \tag{11}$$

where: H is the hidden layer's neuronal number, m is the input layer's neuronal number, n is the output layer's neuronal number, and a is an integer between 1 and 10 [15]. Therefore, the value range of H is 3~12.

As can be seen from Fig. 3, when the number of neurons in the hidden layer is 7, the mean square error of the corresponding training set reaches the minimum, and its value is 0.02622, so the optimal number of neurons in the hidden layer is 7.

4.2.2 Optimize Algorithm Parameter Setting

From the above analysis, it can be seen that the BPNN model's network structure is 7-7-1. The optimization algorithm's initialization parameter settings are shown in Table 2. Among them, the fitness curve of the ISSA-BPNN model in training is shown in Fig. 4.
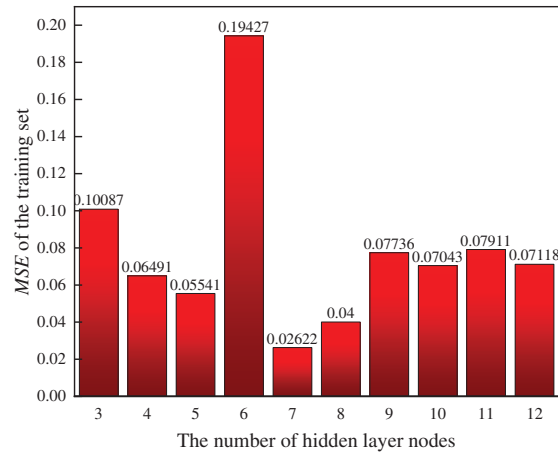
Figure 3: The MSE of the training set at different H values

Table 2: Initialization parameter setting of the optimization algorithm

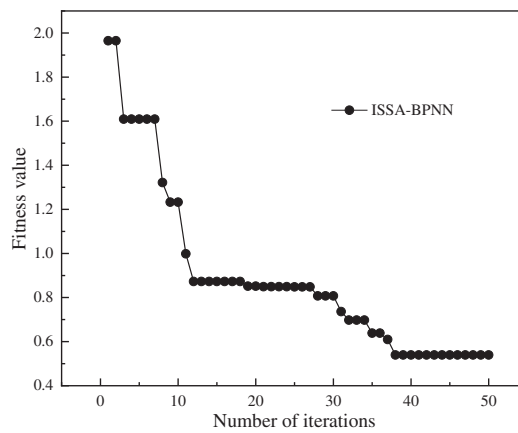| Optimization algorithm	Parameter	Value
GA	Population size	30
	Maximum generations	50
	Crossover fraction	0.8
	Migration fraction	0.2
SSA/ISSA	Population size	30
	Maximum generations	50
	Proportion of discoverers	0.7
	Proportion of guards	0.2
	ST	0.6

Figure 4: Convergence curve of ISSA-BPNN fitness

4.3 Model Forecast Results and Analysis

The prediction results of BPNN, GA-BPNN, SSA-BPNN, and ISSA-BPNN models for pipeline failure pressure are shown in Table 3 and Fig. 5, and the relative error is shown in Fig. 6. The results show that the predicted results of ISSA-BPNN model are closer to the experimental values than those of the other models. Compared with the single BPNN model, the error interval of the BPNN model optimized by the algorithm is greatly reduced, which improves the overall prediction accuracy of the model.

Table 3: Forecast results statistics table

Number	P_F	BPNN		GA-BPNN		SSA-BPNN		ISSA-BPNN	
		$\hat{P}_F$	R_e (%)	$\hat{P}_F$	R_e (%)	$\hat{P}_F$	R_e (%)	$\hat{P}_F$	R_e (%)
1	12.13	12.84	5.82	12.27	1.12	12.27	1.12	12.00	1.08
2	11.92	12.30	3.16	11.56	2.98	12.33	3.44	11.72	1.71
3	11.91	12.26	2.98	11.32	4.98	12.23	2.73	11.69	1.86
4	11.99	12.18	1.61	11.16	6.91	12.01	0.20	11.60	3.27
5	11.30	11.77	4.17	10.70	5.30	10.66	5.65	10.95	3.09
6	13.40	11.63	13.21	14.64	9.28	13.81	3.08	13.69	2.20
7	15.80	14.40	8.86	15.73	0.42	16.58	4.96	17.12	8.36
8	11.25	15.02	33.55	12.64	12.32	12.13	7.84	12.29	9.24
9	8.00	10.64	32.99	9.92	23.98	6.69	16.42	7.87	1.67
10	8.40	10.49	24.87	10.40	23.77	7.94	5.52	8.90	6.01
11	11.55	11.37	1.53	11.60	0.41	11.39	1.38	11.92	3.20
12	27.50	24.76	9.98	25.27	8.11	26.42	3.91	26.19	4.75
13	24.30	23.82	1.99	24.11	0.78	24.98	2.78	24.86	2.30
14	21.80	21.72	0.36	21.70	0.46	22.41	2.79	22.32	2.40
15	19.80	19.38	2.12	19.52	1.41	20.44	3.25	20.22	2.11
16	16.50	12.17	26.24	16.11	2.38	16.93	2.60	16.73	1.42

Note: Where: R_e is the relative error.

The above evaluation indicators evaluate the prediction effect of 4 pipeline failure pressure models (BPNN, GA-BPNN, SSA-BPNN, and ISSA-BPNN), and the results are shown in Table 4 and Figs. 7–10. The prediction accuracy of BPNN model is the lowest, MAE, $RMSE$, $MAPE$, and R^2 are 1.3755, 1.9107, 10.8404% and 0.8895%, respectively, which are the worst among the prediction models. After the BP network is optimized by GA, SSA and ISSA, the prediction error is obviously reduced. Among them, ISSA-BPNN model has the best prediction effect, and its MAE, $RMSE$, $MAPE$, and R^2 are 0.5002, 0.6240, 3.4177% and 0.9980%, respectively, which are the best prediction models. Compared with the SSA-BPNN model, the ISSA-BPNN model has further improved in error size, dispersion degree, and prediction accuracy. It is proved that the introduction of a Logistic chaotic map really improves the quality of the initial sparrow algorithm population solution, and effectively improves the global search ability and prediction performance of the algorithm.
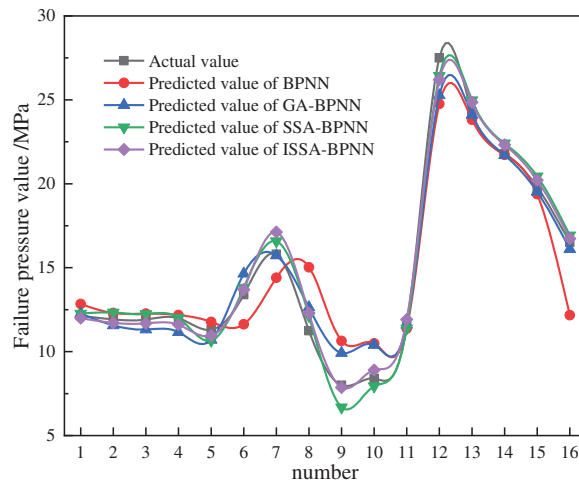
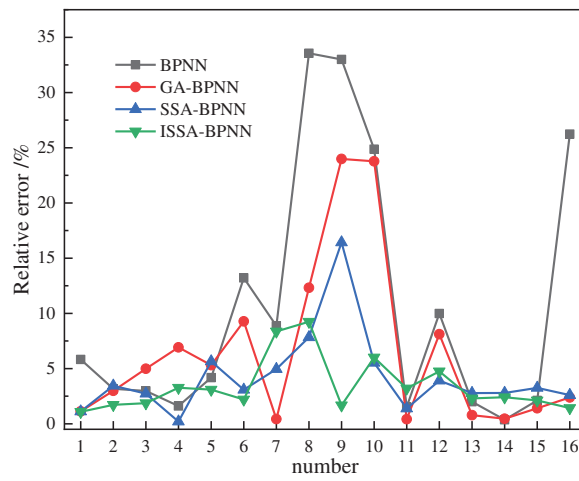**Figure 5:** Comparison of model prediction results

Figure 6: Relative error of prediction results

Table 4: Evaluation indicators statistics table

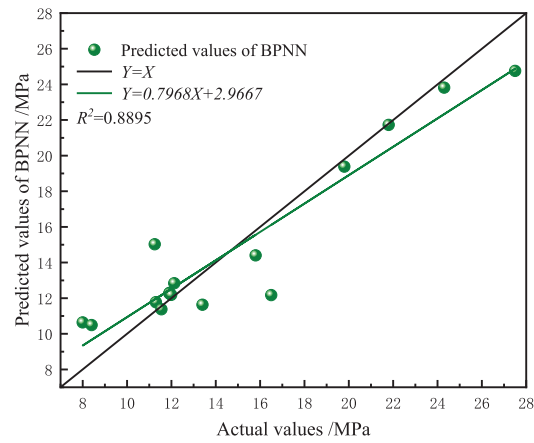| Model	*MAE*	*RMSE*	*MAPE* (%)	*R²*
BPNN	1.3755	1.9107	10.8404	0.8895
GA-BPNN	0.7728	1.0588	6.5391	0.9722
SSA-BPNN	0.5612	0.6524	4.2292	0.9875
ISSA-BPNN	0.5002	0.6240	3.4177	0.9880

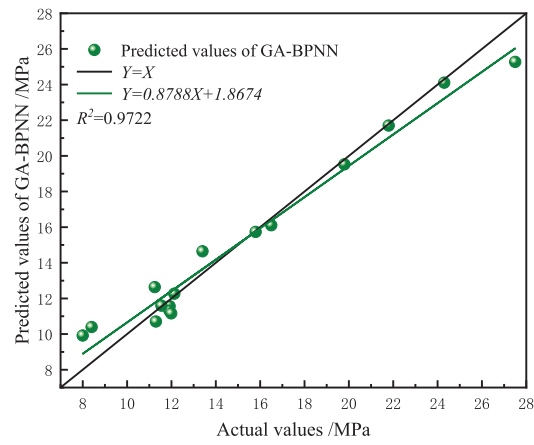**Figure 7:** BPNN prediction results in linear fitting graph

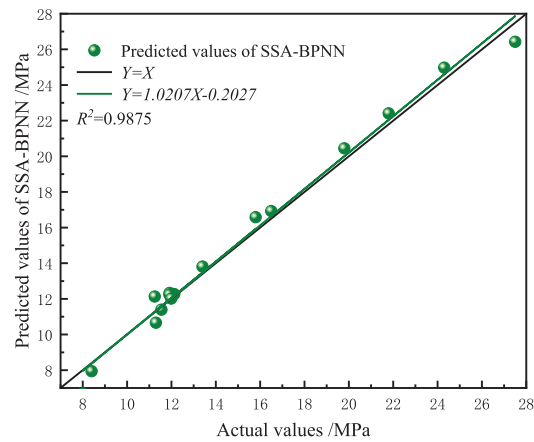**Figure 8:** GA-BPNN prediction results in linear fitting graph

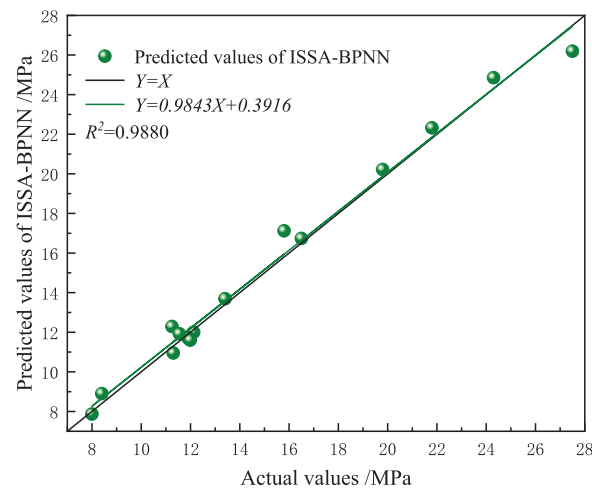**Figure 9:** SSA-BPNN prediction results in linear fitting graph

Figure 10: ISSA-BPNN prediction results in linear fitting graph

5 Conclusion

The fundamental prediction model in this research is BPNN, which is optimized using a variety of optimization techniques and models that are established. Using a model that takes into account seven factors that affect the pipeline's failure pressure, the failure pressure is predicted based on 61 sets of experimental data of pipeline blasting. The following is a summary of the research's results:

(1) The population of SSA is initialized by a Logistic chaotic map strategy, and ISSA is established. The ISSA algorithm is used to optimize the weights and thresholds of the BP neural network, and the ISSA-BPNN pipeline failure pressure prediction model is established.

(2) By comparing four kinds of pipeline failure pressure prediction models, the performance order is as follows: BPNN < GA-BPNN < SSA-BPNN < ISSA-BPNN. Among them, the *MAPE* of the ISSA-BPNN model is 3.4177%, and the R^2 is 0.9880, both of which are superior to its comparison model. It proves that the ISSA-BPNN prediction model has high accuracy and strong robustness, and this model can provide support for pipeline inspection and maintenance.

Author Contributions: Study conception and design: Qi Zhuang. Data collection: Dong Liu and Zhuo Chen. Results analysis and interpretation: Qi Zhuang and Dong Liu. All authors reviewed the results and approved the final version of the manuscript.

Availability of Data and Materials: 61 sets of experimental data of pipeline blasting with defects come from reference [9]. https://doi.org/10.1016/j.oceaneng.2019.106497.

Conflicts of Interest: The authors declare that they have no conflicts of interest to report regarding the present study.

References

1. Chen, C., Li, C., Reniers, G., Yang, F. Q. (2021). Safety and security of oil and gas pipeline transportation: A systematic analysis of research trends and future needs using WoS. *Journal of Cleaner Production, 279,* 1–13.

2. Gao, J., Tian, Y., Han, K. J. (2021). Status quo and construction development trend of China's four major oil and gas channels. *China Oil & Gas, 28(6),* 41–47.

3. Miao, X. Y., Zhao, H., Gao, B. X., Song, F. L. (2023). Corrosion leakage risk diagnosis of oil and gas pipelines based on semi-supervised domain generalization model. *Reliability Engineering and System Safety, 238,* 1–10.

4. Dao, U., Sajid, Z., Khan, F., Zhang, Y., Tran, T. (2023). Modeling and analysis of internal corrosion induced failure of oil and gas pipelines. *Reliability Engineering and System Safety, 234,* 1–15.

5. Lam, C. Z. W. (2016). Statistical analyses of incidents on onshore gas transmission pipelines based on PHMSA database. *International Journal of Pressure Vessels and Piping, 145,* 1–11.

6. Seyed Saleh, M., Ali Shaghaghi, M. (2020). Failure pressure estimation error for corroded pipeline using various revisions of ASME B31G–ScienceDirect. *Engineering Failure Analysis, 109,* 1–14.

7. Bao, J., Zhou, W. (2020). Influence of the corrosion anomaly class on predictive accuracy of burst capacity models for corroded pipelines. *International Journal of Geosynthetics and Ground Engineering, 6(4),* 1–12.

8. British Standards Institution (2007). *Guide to methods for assessing the acceptability of flaws in metallic structures,* vol. 165, pp. 1–11. Bs7910 British Standards.

9. Gao, J., Yang, P., Li, X., Zhou, J., Liu, J. K. (2019). Analytical prediction of failure pressure for pipeline with long corrosion defect. *Ocean Engineering, 191,* 106491–106497.

10. Chen, Y. F., Zhang, H., Zhang, J., Liu, X. B., Li, X. et al. (2015). Failure assessment of X80 pipeline with interacting corrosion defects. *Engineering Failure Analysis, 47,* 67–76.

11. Huang, Y., Qin, G. J., Hu, G. (2022). Failure pressure prediction by defect assessment and finite element modelling on pipelines containing a dent-corrosion defect. *Ocean Engineering, 262(2),* 1–14.

12. Liu, P., Han, Y., Tian, Y. (2021). Residual strength prediction of pipeline with single defect based on SVM algorithm. *Journal of Physics Conference Series, 1944(1),* 012019.

13. Jiang, J. X., Zhang, H., Zhang, D., Ji, B. L., Wu, K. et al. (2022). Fracture response of mitred X70 pipeline with crack defect in butt weld: Experimental and numerical investigation. *Thin-Walled Structures, 177,* 1–11.

14. Jiang, S. Q., Shi, B. (2023). Prediction of failure pressure of corroded pipeline based on ISSA-ELM model. *Hot Working Technology, 52(12),* 70–75.

15. Xu, L. S., Ling, X., Ma, J. J., Ma, H. Q., Fu, X. H. (2021). Prediction on failure pressure of pipeline containing corrosion defects based on DE-BPNN. *Journal of Safety Science and Technology, 17(3),* 91–96.

16. Zhang, T. Y., Shuai, J., Shuai, Y., Hua, L. Y., Xu, K. et al. (2023). Efficient prediction method of triple failure pressure for corroded pipelines under complex loads based on a backpropagation neural network. *Reliability Engineering and System Safety, 231,* 1–12.

17. Li, X. L., Jing, H. M., Liu, X. Y., Chen, G. T., Han, L. F. (2023). The prediction analysis of failure pressure of pipelines with axial double corrosion defects in cold regions based on the BP neural network. *International Journal of Pressure Vessels and Piping, 202,* 104907.

18. Rumelhart, D. E., Hinton, G. E., Williams, R. J. (1986). Learning internal representation by back-propagation errors. *Nature, 323,* 533–536.

19. Xue, J., Shen, B. (2020). A novel swarm intelligence optimization approach: Sparrow search algorithm. *Systems Science & Control Engineering, 8(1),* 22–34.

20. Zheng, Y. Z., Li, L., Qian, L., Cheng, B. S., Hou, W. B. et al. (2023). Sine-SSA-BP ship trajectory prediction based on chaotic mapping improved sparrow search algorithm. *Sensors, 32(2),* 704.